

Gyroradius Scaling of Electron and Ion Transport

C. C. Petty, T. C. Luce, R. I. Pinsker, K. H. Burrell, S. C. Chiu, P. Gohil, R. A. James,* and D. Wròblewski*

General Atomics, San Diego, California 92186-9784

(Received 18 April 1994)

The scaling of heat diffusion with relative gyroradius ρ_* is measured on the DIII-D tokamak using dimensionally similar discharges. For the first time, a two-fluid transport analysis allows the ρ_* scaling of the electron and ion fluids to be determined separately. The electron diffusivity is found to scale like $\chi_e \propto \chi_B \rho_*^{1.1 \pm 0.3}$ (gyro-Bohm-like) while the ion diffusivity is found to scale like $\chi_i \propto \chi_B \rho_*^{-0.5 \pm 0.3}$ (Goldston-like). The scaling of the global confinement time and the effective diffusivity can vary from gyro-Bohm-like to Bohm-like depending upon whether the electrons or ions dominate the heat transport.

PACS numbers: 52.25.Fi, 52.30.-q, 52.55.Fa

The diffusion of heat across magnetic field lines is of fundamental importance to magnetic confinement fusion research. It has been known for many years that heat diffusion in tokamaks and stellarators is much faster than allowed by collisions alone [1], a phenomenon commonly referred to as anomalous heat transport. Although it is widely assumed that some form of plasma turbulence is responsible for anomalous transport, the specific nature is still unknown. It has been recently argued, however, that if the scaling of anomalous transport with relative gyroradius can be determined experimentally, then existing fusion experiments can be scaled to larger ignition devices even without a complete understanding of the process of turbulent diffusion [2].

The relative gyroradius is defined by $\rho_* = \rho_s/a$, where ρ_s is the Larmor radius and a is the plasma minor radius. Using the scale invariance approach to confinement scaling [3,4], and following the example of previous similarity scaling experiments [2,5–11], the thermal diffusivity can be expressed in a dimensionally correct form

$$\chi = \chi_B \rho_*^{x_\rho} F(\nu_*, \beta, q_\psi, T_e/T_i, \alpha_n, \alpha_T, \dots), \quad (1)$$

where $\chi_B = cT_e/eB$, $\nu_* \sim q_\psi n/T^2$, $\beta \sim nT/B^2$, and $\alpha_{n,T} = -(a^2 - r^2)/2rL_{n,T}$. For these relations q_ψ is the safety factor, n is the plasma density, T is the electron or ion temperature, B is the magnetic field strength, and L is the density or temperature scale length. One could interpret the exponent x_ρ as indicating the characteristic turbulence wavelength λ : (a) $x_\rho = 1$ implies $\lambda \sim \rho_s$ which is called gyro-Bohm-like scaling, (b) $x_\rho = 0$ implies $\lambda \sim a$ which is called Bohm-like scaling, and (c) $x_\rho = -1$ implies $\lambda \gg a$ which could arise from having stochastic fields throughout the plasma [8]. Theoretical studies of anomalous diffusion have primarily focused on the first case, turbulence generated by small-scale instabilities.

Discharges which have identical values for all dimensionless parameters of interest except the relative gyroradius are referred to as being “dimensionally similar.” Comparing dimensionally similar discharges of the same size but of different magnetic field allows the exponent x_ρ to be determined from Eq. (1), since the unknown function

F remains a fixed constant. In order to keep ν_* and β constant while varying B , the density and temperature must be scaled as $n \propto B^{4/3}$ and $T \propto B^{2/3}$. Thus for dimensionally similar discharges the thermal diffusivity has the simple scaling

$$\chi \propto B_T^{-(1+2x_\rho)/3}. \quad (2)$$

Previous experiments which used dimensionally similar discharges to determine x_ρ for tokamaks and stellarators have given conflicting results. In tokamak experiments using ion cyclotron heating (ICH) or neutral beam injection (NBI) heating, it was found that the effective diffusivity followed Bohm-like scaling [6–9], although in experiments with NBI heating on DIII-D it was not possible to distinguish between Bohm-like and gyro-Bohm-like transport scaling [5]. Experiments on stellarators using electron cyclotron heating (ECH), however, showed that the confinement scaling was gyro-Bohm-like [10,12]. Direct electron heating experiments on DIII-D also found gyro-Bohm-like scaling of global confinement [11]. Since the global heat conduction for the stellarator experiments was dominated by electrons (due to ECH), while for the tokamak experiments the ion heat conduction was significant (due to ICH and NBI), one may wonder if the conflicting ρ_* scaling results of tokamaks and stellarators may be due to different transport scalings of electrons and ions.

The dimensionally similar discharge experiments reported in this Letter are the first to separate the electron and ion fluids in the analysis in order to determine the ρ_* scaling of transport for each fluid. These experiments were performed on the DIII-D tokamak, typical parameters for which are major radius $R = 1.7$ m, minor radius $a = 0.6$ m, and elongation $\kappa = 1.8$. The plasmas analyzed in this Letter were all specifically generated for these dimensionally similar discharge experiments, with single-null-divertor configuration and fueling by deuterium gas puffing or deuterium NBI. The tokamak was operated in the L -mode scaling regime due to the difficulty in controlling the plasma density in the H -mode regime. The electron density and temperature profiles were measured using Thomson scattering, CO₂ interferometers, and electron cyclotron emission. The ion temperature was found

from charge exchange recombination emission of carbon impurities. The Z_{eff} profiles were determined from visible bremsstrahlung light measured with a photodiode array.

For DIII-D, two forms of central radio-frequency (rf) heating are available to directly heat electrons: 60 GHz ECH and 60 MHz fast wave. The ECH is resonant centrally at 2 T for fundamental absorption and 1 T for second harmonic absorption. Highly efficient direct electron heating near the plasma center by fast waves has been demonstrated previously on DIII-D for the range of electron temperatures obtained in these experiments [13]. Since the hydrogen fraction is measured to be less than 1% for these experiments, second-harmonic hydrogen absorption of the fast wave at 2 T is small compared to direct electron absorption. In some experiments reported in this Letter, deuterium NBI was used as an alternative to rf heating.

The engineering parameters for three pairs of dimensionally similar discharges, two with rf heating and one with NBI heating, are shown in Table I. The fast particle contributions are not included in the values for the stored energy W and confinement time τ_E . The kinetic and equilibrium stored energies are in good agreement for these discharges. The radial profiles of six important dimensionless parameters are shown in Fig. 1 for the dimensionally similar discharges of case (b). The error bars for Figs. 1(a)–1(d) are ascertained by varying the experimental profiles individually by their 1σ uncertainties and re-evaluating the parameters; the errors are combined assuming they are uncorrelated. The error bars for Figs. 1(e) and 1(f) are ascertained by perturbing the spline fit to the profile at the knot locations (one at a time) by its 1σ uncertainty and recalculating the scale length; the errors are combined by applying standard propagation of errors including the covariance. The relative gyro-radius for this pair of discharges is varied by a factor of 1.6 across the plasma while all the other dimensionless parameters are held nearly constant (considering the three pairs of dimensionally similar discharges as a whole, there are no systematic variations in the dimensionless parameters other than in Z_{eff} and ρ_* itself). Although not shown, the profiles of magnetic shear, q_ψ , and α_{T_i} are

TABLE I. Engineering parameters for three pairs of dimensionally similar discharges.

Shot No.	(a)		(b)		(c)	
	78328 ECH	78316 ECH, FW	78281 ECH	78106 ECH, FW	78283 NBI	78109 NBI
B_T (T)	1.0	2.0	1.0	2.0	1.0	2.0
I_p (MA)	0.5	1.0	0.5	1.0	0.5	1.0
q_ψ^{95}	4.8	5.0	5.8	5.9	5.8	5.8
\bar{n} (10^{19} m^{-3})	1.0	2.6	1.4	3.8	1.2	3.1
W (kJ)	42	175	44	179	44	178
Z_{eff}	3.2	2.3	2.5	2.1	3.0	1.6
P_{tot} (MW)	1.1	2.2	0.6	2.0	0.6	1.9
τ_E (msec)	39	81	74	91	74	93

also well matched as is the normalized power deposition profile outside $r/a = 0.4$.

The thermal diffusivities for these discharges are determined from a radial power balance analysis $\nabla \cdot (\mathbf{q} + 5/2\Gamma T) = Q$ (in steady state), where q is the radial heat flux, Γ is the particle flux, and the heat sources and sinks are combined into Q . The transport computations are done by the ONETWO code [14], which uses the measured electron and ion temperatures, electron density, effective ion charge Z_{eff} , and radiated power, along with the plasma current profile and magnetic geometry. The plasma profiles are analyzed after 400 msec of auxiliary heating, by which time steady-state conditions ($\dot{W} = 0$, $\dot{l}_i = 0$) have been reached. The radial heat flux is assumed to be purely diffusive in this analysis ($q = -n\chi\nabla T$).

For case (a), the ρ_* scaling of the electron diffusivity is gyro-Bohm-like, $x_\rho \approx 1$, while the ρ_* scaling of the ion diffusivity is intermediate between Bohm-like and stochastic, $x_\rho \approx -\frac{1}{2}$. This is determined from the ratio of the electron and ion diffusivities for the 2 and 1 T discharges, shown in Fig. 2, in conjunction with Eq. (2). The indicated error bars are from the combined random errors in the quantities q/nT and L_T^{-1} . The error in q/nT is determined by varying the experimental profiles individually by their 1σ uncertainties and recalculating the power balance; the errors are combined assuming they are uncorrelated. The error in L_T^{-1} is determined using the same method as described previously for Fig. 1. Results for the plasma edge are not shown in Fig. 2, since the uncertainties in the electron and ion diffusivities increase

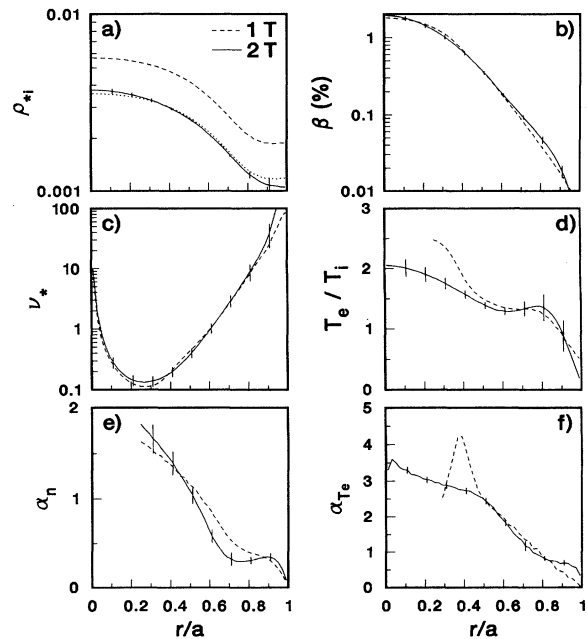


FIG. 1. Nondimensional parameters for case (b), a pair of dimensionally similar discharges with central rf heating. The dotted line in (a) shows the 1 T relative gyroradius scaled to the 2 T discharge.

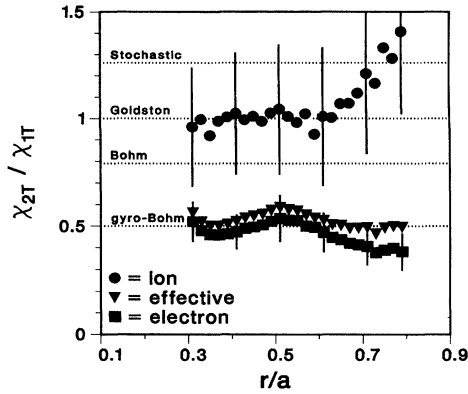


FIG. 2. Ratio of the electron, ion, and effective diffusivities for the 2 and 1 T discharges of case (a).

rapidly in that region, making a two-fluid transport analysis untenable. The plasma center is also excluded due to the effects of sawteeth (the sawtooth mixing radius is located at $r/a = 0.3$) and differences in the normalized power deposition profiles near the magnetic axis. It is interesting to note that the scaling of the ion transport is the same as that expected from the Goldston scaling relation [15], $\tau_E \propto I_p \bar{n}^0 B_T^0 P_{tot}^{-1/2}$; therefore, the scaling $x_\rho = -\frac{1}{2}$ will be referred to as Goldston-like. Also shown in Fig. 2 is the effective thermal diffusivity, which is calculated from

$$\chi_{eff} = -\frac{q_e + q_i}{n_e \nabla T_e + n_i \nabla T_i}. \quad (3)$$

Previous dimensionally similar discharge experiments on tokamaks analyzed χ_{eff} only [2,5-9,11]. The effective diffusivity in Fig. 2 is observed to scale as gyro-Bohm. From Table I, the global confinement time is found to scale like $\tau_E \propto B_T^{1.05}$, which is also gyro-Bohm-like. The reason that the effective diffusivity (and thus the global confinement time) closely follows the ρ_* scaling of the electrons and not the ions is because the electron heat flux is 3 to 10 times the ion heat flux, due to direct electron heating and weak ion-electron collisional coupling at these low densities.

For case (b), the global confinement time exhibits Bohm-like scaling, $\tau_E \propto B_T^{0.29}$, instead of gyro-Bohm-like scaling as in case (a). The thermal diffusivities for case (b) are shown in Fig. 3; the effective diffusivity is also seen to scale close to Bohm-like. However, the ρ_* scaling of the electron and ion diffusivities is unchanged between Figs. 2 and 3: the electron diffusivity still scales as gyro-Bohm while the ion diffusivity still scales as Goldston. The difference is that at the higher densities of case (b) the electron-ion collisional coupling is much stronger, resulting in the ions conducting nearly half of the heat out of the plasma. Therefore, the scaling of the effective diffusivity, and the scaling of the global confinement time, is an average of the electron and ion scalings. Since Bohm scaling happens to fall about halfway between gyro-Bohm and Goldston scaling, the scaling of the effective diffusivity appears to be Bohm-like

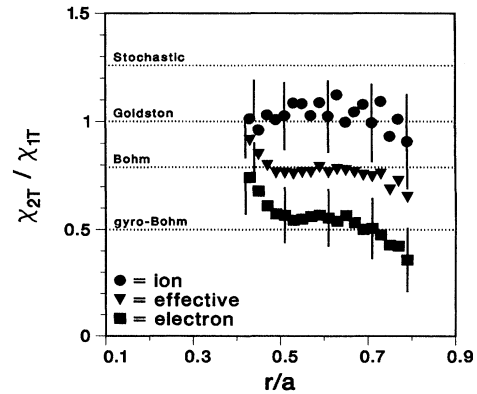


FIG. 3. Ratio of the electron, ion, and effective diffusivities for the 2 and 1 T discharges of case (b).

even though neither species has Bohm-like scaling. This demonstrates the pitfall in using the effective diffusivity or global confinement time to determine transport scaling, since in reality one is measuring the average of possibly different electron and ion scalings.

If the ρ_* scaling of the electron and ion fluids displayed in Figs. 2 and 3 is an intrinsic property of anomalous transport, then the result should not depend on the method of auxiliary heating. This hypothesis was tested by studying dimensionally similar discharges using NBI heating instead of rf heating. For case (c) with NBI heating, the global confinement time is seen to scale like $\tau_E \propto B_T^{0.33}$, which is Bohm-like. The thermal diffusivities for case (c) are shown in Fig. 4. The electron and ion transport are found to scale as gyro-Bohm and Goldston, respectively, the same result as obtained with rf heating. Since the electron and ion heat conduction are both significant for these NBI discharges, the effective diffusivity scales as the average of the electron and ion transport, which is coincidentally close to Bohm-like. It is noteworthy for the supposition of classical collisional coupling that the ρ_* scaling of the ion fluid is the same regardless of the method of auxiliary heating, since for cases (a) and (b) the ion heating is due

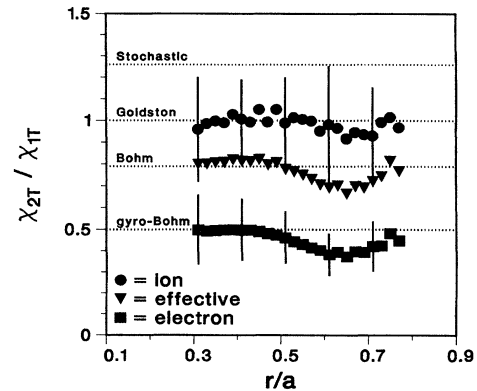


FIG. 4. Ratio of the electron, ion, and effective diffusivities for the 2 and 1 T discharges of case (c).

to ion-electron collisional exchange, whereas for case (c) direct beam ion heating is dominant.

The relationships between the global confinement time, the local thermal diffusivities, and the fraction of electron heat conduction for the dimensionally similar discharges of Table I are shown in Fig. 5. The exponent x_τ is defined by $\tau_E \propto B_T^{-1} \rho_*^{x_\tau}$, where $x_\tau = -3$ for gyro-Bohm-like scaling and $x_\tau = -2$ for Bohm-like scaling. Figure 5 shows that the scalings of the electron and ion diffusivities are independent of the fraction of electron heat conduction, and thus may be considered intrinsic transport properties. However, the scalings of the effective diffusivity and the global confinement time change from gyro-Bohm-like, when the electron heat-conduction fraction is near 1, to Bohm-like, when the electrons and ions participate more equally in the heat conduction. Therefore, these scalings are not intrinsic. Combining the three separate measurements of the ρ_* scaling in Fig. 5 into a final result yields $\chi_\rho = 1.1 \pm 0.3$ for electron transport and $\chi_\rho = -0.5 \pm 0.3$ for ion transport.

In conclusion, gyroradius scaling experiments on the DIII-D tokamak have shown that the electron diffusivity scales like $\chi_e \propto \chi_B \rho_*^{1.1 \pm 0.3}$ (gyro-Bohm-like) while the ion diffusivity scales like $\chi_i \propto \chi_B \rho_*^{-0.5 \pm 0.3}$ (Goldston-like). This result is obtained with either central rf heating (ECH and fast wave) or NBI heating. Although Z_{eff} is not held constant in these ρ_* scans, no correlation is observed between the variation in Z_{eff} and the change in transport. The gyro-Bohm-like scaling of χ_e is the expected result for small-scale turbulence, but at present there is no theo-

retical explanation for the ρ_* scaling of χ_i . Although this transport analysis assumes a purely diffusive heat flux, the ρ_* scaling of the thermal diffusivities is not affected by the presence of a nondiffusive heat flux as long as the ratio of diffusive to nondiffusive transport is independent of ρ_* . If this is not the case, then the measured transport scaling with ρ_* is actually an average of the diffusive and nondiffusive scalings. Since the electron and ion fluids have different ρ_* scalings, the effective diffusivity and the global confinement scalings are found to vary from gyro-Bohm-like to Bohm-like depending upon whether the electrons or ions dominate the heat conduction. This property explains the different ρ_* scaling results reported in the literature for dimensionally similar discharges, where ECH in stellarators [10,12] and tokamaks [11] had gyro-Bohm-like confinement scaling, whereas ICH and NBI heating in tokamaks [6–9] had Bohm-like confinement scaling. Therefore, it is evident that the effective diffusivity and global confinement time do not always adequately determine the transport properties of the component species.

This work is supported by the U.S. Department of Energy under Contract No. DE-AC03-89ER51114 and No. W-7405-ENG-48. We would like to thank J. S. deGrassie, C. B. Forest, R. J. La Haye, and A. W. Leonard for being the tokamak physics operators for these experiments and M. E. Austin for analyzing the ECE data.

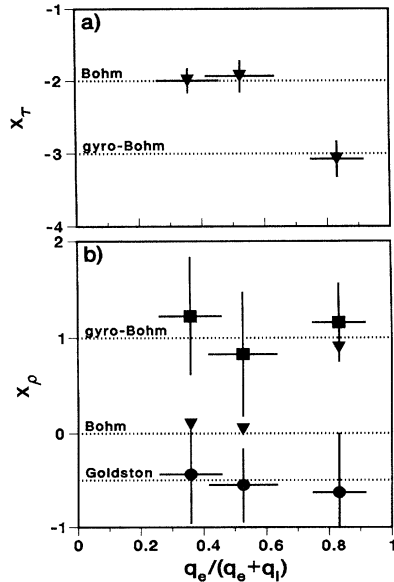


FIG. 5. Gyroradius scaling exponents for (a) global confinement, (b) electron (■), ion (●), and effective (▼) diffusivities as a function of the fraction of heat conduction in the electron channel. The horizontal bars indicate the variation in the electron heat conduction fraction across the plasma radius.

*Permanent address: Lawrence Livermore National Laboratory, Livermore, California 94550.

- [1] B. B. Kadomtsev and O. P. Pogutse, Nucl. Fusion **11**, 67 (1971).
- [2] R. E. Waltz, J. C. DeBoo, and M. N. Rosenbluth, Phys. Rev. Lett. **65**, 2390 (1990).
- [3] B. B. Kadomtsev, Sov. J. Plasma Phys. **1**, 295 (1975).
- [4] J. W. Connor and J. B. Taylor, Nucl. Fusion **17**, 1047 (1977).
- [5] R. E. Waltz, J. C. DeBoo, and T. H. Osborne, Nucl. Fusion **32**, 1051 (1992).
- [6] S. D. Scott *et al.*, in Proceedings of the 14th International Conference on Plasma Physics and Controlled Nuclear Fusion Research Würzburg, 1992 (International Atomic Energy Agency, Vienna, 1993), Vol. **3**, p. 427.
- [7] F. W. Perkins *et al.*, Phys. Fluids B **5**, 477 (1993).
- [8] J. P. Christiansen *et al.*, Plasma Phys. Controlled Fusion **34**, 1881 (1992).
- [9] J. P. Christiansen *et al.*, Nucl. Fusion **33**, 863 (1993).
- [10] U. Stroth *et al.*, Phys. Rev. Lett. **70**, 936 (1993).
- [11] C. C. Petty, T. C. Luce, and R. I. Pinsky, in Proceedings of the Tenth Topical Conference on Radio-Frequency Power in Plasmas Boston, MA, 1993 (American Institute of Physics, New York, 1994), p. 165.
- [12] J. B. Wilgen *et al.*, Phys. Fluids B **5**, 2513 (1993).
- [13] C. C. Petty *et al.*, Phys. Rev. Lett. **69**, 289 (1992).
- [14] W. W. Pfeiffer *et al.*, General Atomics Report No. GA-A16178, 1980 (unpublished).
- [15] R. J. Goldston, Plasma Phys. Controlled. Fusion **26**, 87 (1984).